ORIGINAL PAPER

H. Sowa · H. Ahsbahs · W. Schmitz

X-ray diffraction studies of millerite NiS under non-ambient conditions

Abstract The high-pressure behaviour of millerite NiS up to 34.7 GPa was studied using single-crystal X-ray diffraction techniques. Under ambient pressure, 8.3, 19.2 and 26.8 GPa crystal-structure determinations were performed. No phase transition was observed and the fit of the Birch-Murnaghan equation of state gave a bulk modulus $K = 111(1)$ GPa and a pressure derivative $K' = 5.0(1)$ at high pressure and room temperature. The high-temperature modification of NiS belongs to the NiAs type and has the smaller volume per formula unit. High-pressure–high-temperature X-ray diffraction studies on NiS powder indicate that the transition temperature is strongly dependent on pressure. Owing to the higher compressibility of millerite compared with that of the high-temperature phase, it is assumed that the NiAs-type is not the stable phase at high pressures.

Keywords Millerite · NiS · High pressure · Crystal structure · High temperature

H. Sowa (✉)
Institut für Angewandte Geowissenschaften,
Allgemeine und Angewandte Mineralogie,
Technische Universität BH1,
Ernst-Reuter-Platz 1, 10587 Berlin
e-mail: heidrun.sowa @t-online.de

H. Ahsbahs
Institut für Mineralogie,
Petrologie und Kristallographie und Wissenschaftliches Zentrum für Materialwissenschaften,
Universität Marburg,
Hans-Meerwein-Straße,
35032 Marburg

W. Schmitz
Institut für Mineralogie,
Kristallographie und Materialwissenschaft,
Universität Leipzig, Scharnhorststr. 20,
04275 Leipzig

Introduction

NiS is known to be dimorph. Under ambient conditions millerite β-NiS is the stable phase. It shows metallic conductivity and an unusual crystal structure in space group R3m with hexagonal unit-cell parameters $a = 9.607(1)$ Å and $c = 3.143(1)$ Å. All atoms occupy Wyckoff positions 9(b) $x,-x,z$ with $x = -0.0878$, $z = 0.475$ (Ni) and $x = 0.1122$, $z = 0$ (S) (Grice and Ferguson 1974; Rajamani and Prewitt 1974). The arrangement of the sulphur atoms correspond to a slightly distorted homogeneous sphere packing of type 8/3/h7 (Sowa et al. 2003) with eight contacts per sphere and the Ni atoms are located in its fivefold coordinated voids of pyramidal shape (Fig. 1). The Ni atoms form clusters of three atoms with Ni–Ni distances of only 2.53 Å (Ni metal: $d_{Ni-Ni} = 2.49$ Å). That means that each Ni atom has five S and two Ni neighbours, and each S atom is coordinated by five Ni atoms. The only other known compound that crystallizes with this structure type is the mineral mäkinenite γ-NiSe (Vuorelainen et al. 1964).

Using electron spectroscopic measurements and band structure calculations, Krishnakumar et al. (2002) gave a detailed description of the electronic structure of millerite. Their investigations indicate that millerite is a "highly covalent metal".

At high temperatures millerite undergoes a phase transition to a polymorph α-NiS that belongs to the NiAs type ($P6_3/mmc$). For stoichiometric NiS the transition temperature is 379 °C (Kullerud and Yund 1962). At room temperature the lattice parameters of metastable α-NiS are $a = 3.4395(2)$ Å and $c = 5.3514(7)$ Å (Trahan et al. 1970). The Ni atoms occupy Wyckoff positions 2(a) 0,0,0 and the S atoms are located at 2(c) $\frac{1}{3}, \frac{2}{3}, \frac{1}{4}$. The sulphur atoms form a hexagonal close packing and the Ni atoms occupy its octahedral voids. Remarkably, at room temperature the volume per formula unit is smaller for α-NiS (27.4 Å^3) than for the low-temperature modification millerite (28.0 Å^3).
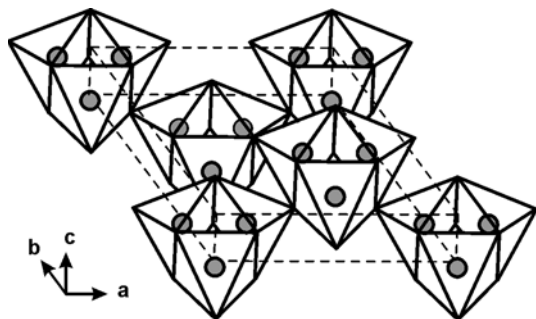
Fig. 1 Connection of the distorted tetragonal NiS₅ coordination pyramids in millerite

Though α-NiS can easily be quenched, it does not occur as a mineral. Owing to its electrical properties at low temperatures this metastable modification of NiS has attracted more attention than millerite (cf. Okamura et al. 1999 and references herein). Under ambient conditions NiAs-type NiS is a paramagnetic metal and it becomes an antiferromagnetic non–metal at 265 °C (Sparks and Komoto 1963). The paramagnetic → antiferromagnetic transition temperature decreases with increasing pressure and above 2 GPa the antiferromagnetic phase does not occur (McWhan et al. 1972). High-pressure investigations up to 50 GPa on NiAs-type NiS were performed by Campbell and Heinz (1993), who did not observe a phase transition up to 45 GPa. Above this pressure, laser heating induced a transformation to an unknown phase. Owing to the negative volume change associated with the millerite-to-NiAs-type transition at ambient pressure the authors assumed that the high-temperature phase should be also the high-pressure phase.

Until now, many AB compounds have been investigated under high pressures but nothing is known about the high-pressure behaviour of millerite. There-fore, the present work aims to obtain information about the pressure-dependent variations of this structure type.

Experimental

For the present investigations natural millerite from Wissen/Sieg (Germany) was used. Electron-microprobe analyses of four crystals show a slight Ni deficiency and only small amounts of Fe and Co. The indicated composition is $Ni_{0.966}Co_{0.004}Fe_{0.002}S$.

High-pressure single-crystal investigations at room temperature

The quality of several single crystals was checked and only untwinned ones that show sharp reflections were used for further investigations. All single-crystal high-pressure experiments (except that at 8.3 GPa) were carried out with a "quadratic" diamond-anvil cell (Ahsbahs 1995) and rhenium gaskets. Compressed helium gas at about 0.2 GPa was loaded into the cell to obtain quasihydrostatic conditions. The pressure was calibrated with the ruby fluorescence method (Piermarini et al. 1975) using the pressure scale of Mao et al. (1986). The precision of the pressure measurements was estimated to be better than ± 0.1 GPa. In a first run, precise unit-cell parameters of millerite were determined on a STOE four-circle diffractometer (MoKα radiation, $\lambda = 0.7107$ Å, graphite monochromator). At various pressures, 10–12 reflections with $9° \leq 2\theta \leq 30°$ were centred at eight equivalent positions according to the method of King and Finger (1979). At 7.5 GPa the crystal was broken into four pieces and the measurements at higher pressures were performed using only the largest one. At 34.7 GPa the reflections became very broad and only eight could be measured. Lattice-parameter refinements performed without constraints led within two estimated standard deviations to angles $\alpha = \beta = 90°$, $\gamma = 120°$ and to cell parameters a = b. The final unit-cell parameters were determined by the vector-least-squares method with constraints (Ralph and Finger 1982). A second very small single crystal (cf. Table 1) was used for the subsequent investigations of the crystal structure of millerite at 19.3 and 26.8 GPa. The measurement at 8.3 GPa was part of a comparative study using single-counter and imaging-plate techniques (Ahsbahs 2004). It was performed using a new type of high-pressure cell developed especially for intensity collections on area-detector

Table 1 Details of data collections and final R values

P (GPa)	0.0001	8.3	19.3	26.8
Crystal size (μm³)	150 × 100 × 20	60 × 45 × 30	35 × 25 × 10	35 × 25 × 10
$2\theta_{max}$ (°)	80	80	80	80
Step width (°)	0.01	0.015	0.015	0.015
Scan with (°)	1 ° + 0.04 tanθ	0.9 ° + 0.04 tanθ	0.9 ° + 0.05 tanθ	0.9 ° + 0.05 tanθ
Counting time per step (s)	1–4	6–30	10–50	10–50
Total number of reflections	397	397	369	364
No. of used reflections	397	392	364	356
No. of independent reflections (total)	260	258	245	239
With $I > 4\sigma(I)$	255	236	199	193
R_{int} (all reflections) (%)	2.98	2.98	3.68	4.11
$wR2$ (all reflections) (%)	3.86	7.22	6.48	6.57
R1 (all reflections) (%)	1.71	3.86	6.49	6.00
R1 ($I > 4\sigma(I)$) (%)	1.64	3.06	3.49	3.50
GooF	1.026	1.148	1.120	1.080

$R_{int} = \sum |F_o{}^2 - F_o{}^2(mean)| / \sum [F_o{}^2]$

$R1 = \sum \|F_o - F_c\| / \sum F_o$

$wR2 = \{\sum [w(F_o{}^2 - F_c{}^2)] / \sum [w(F_o{}^2)]\}^{\frac{1}{2}}$

$w = 1/[\sigma^2(F_o{}^2) + (aP)^2 + bP]$, $P = [2 F_c{}^2 + max(F_o{}^2, 0)]/3$

$GooF = \{\sum [w(F_o{}^2 - F_c{}^2)] / (n-p)\}^{\frac{1}{2}}$, $n =$ number of F,

$p =$ number of l. s. parameters

diffractometers (Ahsbahs 2001). Only one half of this cell contains a beryllium plate. For the present investigation, data were collected with a single counter, and the pressure-transmitting medium was a 4:1 mixture of methanol:ethanol. In all cases, intensity data were collected in the ω-scan technique using the fixed-φ method (Finger and King 1978). In order to keep low the background generated by the beryllium parts of the cell, an edge-formed collimator in front of the counter was used (Ahsbahs 1987; Zhang and Ahsbahs 1998). Owing to the very small crystal sizes, long measuring times (up to 1h per reflection) were necessary. The intensities were corrected with respect to the absorption of the incident and the reflected X-ray beam in the diamond anvils and the beryllium parts of the pressure cell. Sample reflections that overlap with reflections of the diamonds or the ruby crystal were omitted from the datasets. During the data collection under ambient conditions the existence of a pressure cell was simulated to enable a better comparison with the data yielded at high pressure. This technique should minimize differences in the systematic errors caused by the diamond-anvil cell. Corrections for the Lorentz and polarization effects were applied. The program CRYMIS (Kutoglu 1995) was used for the data reduction. Details of the data collections are given in Table 1. The structure refinements were carried out with SHELXL-93 (Sheldrick 1993) with anisotropic displacement factors.

High-temperature investigations on powder at ambient pressure

For the high-temperature studies millerite crystals were finely ground and the powder was mixed 1:1 with silicon powder. The measurements were carried out using a SEIFERT XRD 3000 powder diffractometer (CuKα radiation, $\lambda = 1.5419$ Å) with a position-sensitive detector. At various temperatures up to 450 °C the diffraction patterns were recorded in the range $15° \leq 2\theta \leq 130°$. The heating rate was 2–3 °C min^{-1} and before each measurement the temperature was held for 3 min. The accuracy in temperature was approximately ± 10 °C measured with a precision of ± 2 °C.

### High-pressure–high-temperature investigations on powder

The high-temperature–high-pressure experiments were performed using a water-cooled lever arm diamond-anvil cell (opening angle 30°) with a cylindrical resistance heater around the diamond anvils. In order to produce quasihydrostatic pressures, NaF was employed as the pressure-transmitting medium because it shows only one powder ring within the accessible 2θ range. A 1:2 mixture of fine ground millerite and NaF together with a small ruby sphere was filled into a high-temperature-resistant steel gasket. The temperature was controlled with a NiCr–Ni thermocouple. Powder-diffraction patterns were obtained using a Debye–Scherrer film technique (camera radius 45 mm) with monochromated Mokβ radiation ($\lambda = 0.6323$ Å, focusing Si monochromator). At each pressure, first the sample was heated within 2 h up to the desired temperature, then this temperature was held for 1 h and, subsequently, the sample was cooled down to room temperature within half an hour. After this treatment a film was taken with an exposure time of approximately 16 h. In the following runs the temperature was increased by 10 °C each time until the phase transformation was observed. Since the high-temperature phase does not transform back to millerite on cooling, it was not necessary to perform X-ray diffraction measurements while heating the sample. The transition temperature was determined under ambient conditions at 2.6 and 7.2 GPa, but it has be taken into account that heating gives rise to an increase in pressure so that the accurate transition pressure is unknown. Considering the thermal-expansion coefficients of the sample and the steel gasket, an increase in pressure of approximately 1 GPa seems to be possible.

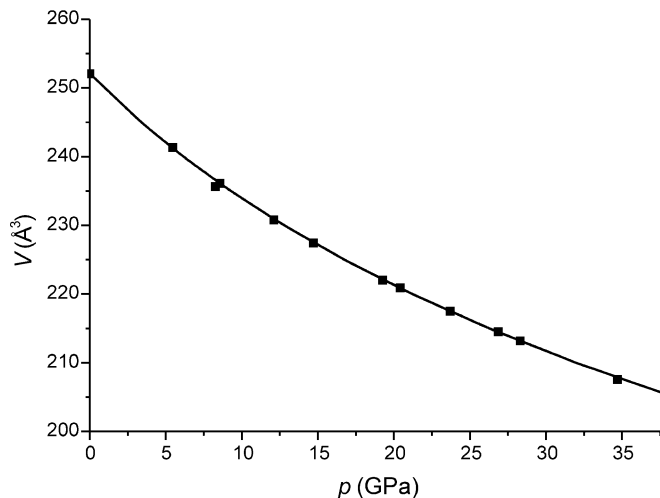**Table 2** Lattice parameters of millerite at various pressures

p (GPa)	a (Å)	c (Å)	V (Å^3)	c/a
0.0001	9.6112(6)	3.1508(5)	252.06(5)	0.3278
5.5	9.469(1)	3.1080(8)	241.35(8)	0.3282
8.3	9.4063(9)	3.0885(7)	236.65(7)	0.3283
8.6	9.396(2)	3.087(2)	236.1(2)	0.3285
12.1	9.325(2)	3.065(1)	230.8(1)	0.3287
14.7	9.278(1)	3.051(1)	227.4(1)	0.3288
19.3	9.2043(5)	3.0263(5)	222.03(4)	0.3288
20.4	9.187(2)	3.022(2)	220.9(1)	0.3289
23.7	9.140(2)	3.006(2)	217.5(2)	0.3289
26.8	9.097(1)	2.9934(9)	214.54(8)	0.3291
28.3	9.078(2)	2.987(1)	213.2(1)	0.3290
34.7	8.994(10)	2.963(9)	207.6(8)	0.3294

Results and discussion

No phase transition could be observed at room temperature up to the highest pressure achieved in the experiments. Table 2 lists the lattice parameters and unit-cell volumes at various pressures. Fitting a third-order Birch–Murnaghan equation of state resulted in $V_o = 252.10(9)$ Å^3 and in a bulk modulus $K = 111(1)$ GPa and its pressure derivative $K' = 5.01(1)$. The
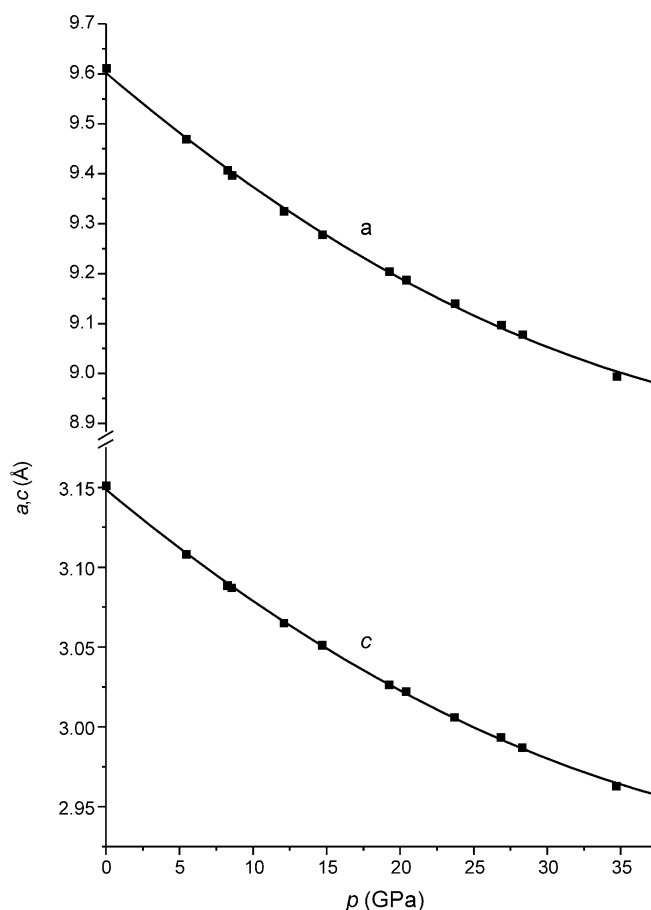
Fig. 2 Hexagonal lattice parameters a and c of millerite versus pressure. The *lines* are guides to the eyes

Fig. 3 Volume V of the hexagonal unit cell of millerite versus pressure

Table 4. Interatomic distances in millerite at various pressures

p (GPa)	0.0001	8.3	19.3	26.8
$d_{(Ni–S)}$ (Å) (1x)	2.266(1)	2.206(2)	2.151(2)	2.120(2)
$d_{(Ni–S)}$ (Å) (2x)	2.277(1)	2.247(2)	2.212(2)	2.196(2)
$d_{(Ni–S)}$ (Å) (2x)	2.362(1)	2.310(2)	2.257(2)	2.229(2)
$d_{(Ni–Ni)}$ (Å) (2x)	2.531(1)	2.485(2)	2.440(2)	2.414(2)
$d_{(S–S)}$ (Å) (2x)	3.151(1)	3.088(1)	3.026(1)	2.993(1)
$d_{(S–S)}$ (Å) (2x)	3.238(1)	3.188(3)	3.130(4)	3.103(3)
$d_{(S–S)}$ (Å) (4x)	3.355(1)	3.275(2)	3.201(2)	3.153(2)
$d_{(S–S)}$ (Å) (4x)	3.817(1)	3.729(1)	3.647(1)	3.601(1)

fitting was weighted by the uncertainties on the pressure and volume measurements (Angel 2002). Figures 2 and 3 display the pressure-induced unit-cell variations. Millerite shows a nearly isotropic compression, therefore the axial ratio c/a does not change remarkably. Positional and atomic displacement parameters yielded from the structure refinements are given in Table 3. The positional parameters vary slightly with increasing pressure, indicating that the deviations from the ideal sulphur sphere packing are reduced. While under ambient conditions the anisotropic displacement parameters of the sulphur atoms are reliable, those at high pressures describe a very flat ellipsoid (cf. Table 3). This effect is probably caused by an undetected systematic error. All bond distances decrease with increasing pressure (Table 4). It is remarkable that the initially shortest Ni–S distance becomes considerably shorter. This is the distance between the Ni atom in the centre and the S atom at the apex of each distorted tetragonal pyramid. The Ni–S distances to the S atoms at the pyramidal basal plane seem to approach equivalent values. The shortest Ni–Ni distances are reduced to $d_{Ni–Ni} = 2.414(2)$ Å at 26.8 GPa. The difference between the two shortest S–S distances becomes smaller at high pressure.

The high-temperature investigations at ambient pressure revealed that the transformation to the NiAs type does not appear abruptly. At 370 °C the strongest reflection 102 of NiAs-type NiS occurred as a very weak peak at about $2\theta = 45.4$ ° (Fig. 4). With increasing temperature the amount of NiAs-type NiS increased, but the transformation was not finished at 400 °C. Therefore, between 380 and 400 °C it was possible to determine the lattice parameters of both phases. At 450 °C only peaks belonging to the high-temperature modification could be detected. As described in the literature (e.g. Kullerud and Yund 1962), this phase can be quenched, and millerite was not recovered at the end of the experiment.

Table 3 Positional and atomic displacement parameters of millerite at various pressures

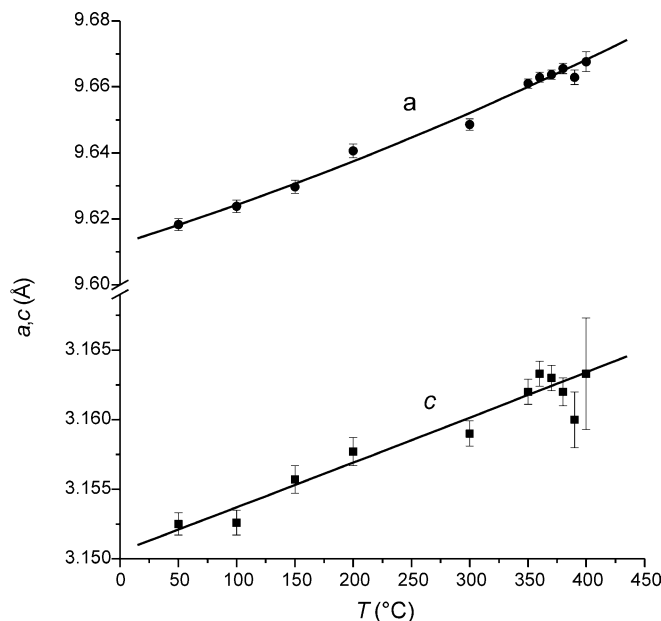| p (GPa)		0.0001	8.3	19.3	26.8
Ni	x	0.91221(2)	0.91195(5)	0.91162(6)	0.91153(6)
	z	0.4802(2)	0.4848(6)	0.4891(7)	0.4918(7)
	U_{11} (Å^2)	0.0060(1)	0.0026(3)	0.0030(3)	0.0047(3)
	U_{33} (Å^2)	0.0071(1)	0.0051(3)	0.0030(3)	0.0049(3)
	U_{23} (Å^2)	−0.00006(6)	−0.0001(2)	−0.0002(2)	−0.0000(1)
	U_{12} (Å^2)	0.0033(2)	0.0014(3)	0.0018(4)	0.0026(4)
	U_{eq} (Å^2)	0.0063(1)	0.0033(2)	0.0028(2)	0.0047(2)
S	x	0.11229(5)	0.1130(1)	0.1133(1)	0.1137(1)
	U_{11} (Å^2)	0.0079(2)	0.0052(5)	0.0053(6)	0.0067(6)
	U_{33} (Å^2)	0.0061(2)	0.0033(5)	0.0030(6)	0.0050(6)
	U_{23} (Å^2)	−0.00040(9)	−0.0002(2)	−0.0001(3)	−0.0002(3)
	U_{12} (Å^2)	0.0055(3)	0.0049(6)	0.0048(7)	0.0059(8)
	U_{eq} (Å^2)	0.0066(1)	0.0036(3)	0.0036(3)	0.0050(3)
Main axes of the displacement parameter ellipsoids (Å^2)					
	Ni	0.0071	0.0051	0.0032	0.0049
		0.0062	0.0027	0.0031	0.0049
		0.0053	0.0023	0.0022	0.0042
	S	0.0089	0.0067	0.0067	0.0084
		0.0064	0.0034	0.0031	0.0051
		0.0044	0.0006	0.0009	0.0015
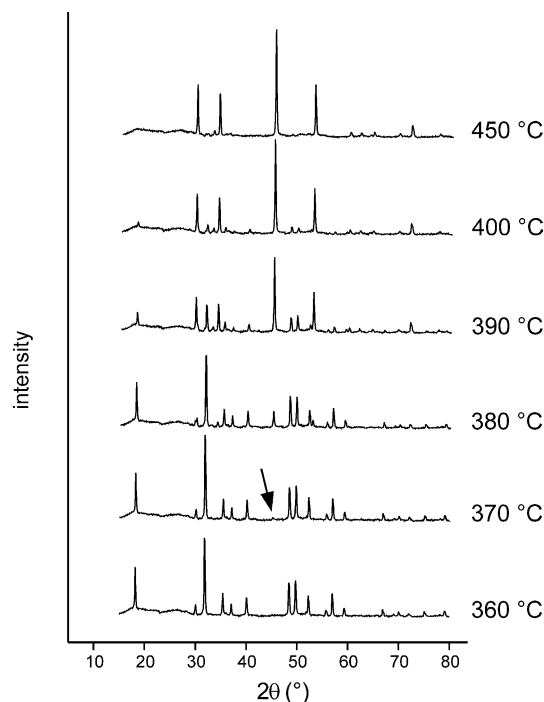
Fig. 4 X-ray powder diffraction patterns of NiS (sample without Si) at various temperatures between 360 and 450 °C with $15 \leq 2\theta \leq 80°$. The *arrow* marks the first occurrence of the strongest peak of NiAs-type NiS

Fig. 5 Hexagonal lattice parameters a and c of millerite at high temperatures. The *lines* are guides to the eyes

With increasing temperature the lattice parameters of millerite increase slightly (Table 5; Fig. 5). The volume per formula unit is lower for the high-temperature phase than for millerite not only under ambient conditions but also at high temperatures (Fig. 6).

A comparison of the crystal structures of both NiS phases at room temperature shows that the averaged S–S distances in NiAs-type NiS are shorter than those in millerite (Table 6), resulting in a denser packing. On the other hand the Ni–S and Ni–Ni distances in millerite are shorter than those in the NiAs-type phase. The interactions between these atoms are assumed to stabilize

millerite at lower temperatures (Grice and Ferguson 1974; Rajamani and Prewitt 1974; Raybaud et al. 1997).

The high-temperature–high-pressure measurements reveal that the temperature for the transition from millerite to NiAs-type NiS decreases drastically with increasing pressure—even if the actual transition pressure was higher than the pressure determined at ambient temperature (see above). Figure. 7 displays the results of these investigations. Regarding these data, it has to be taken into account that—caused by the experimental assembly—the absolute temperature values are not correct. For instance, the thermocouple was welded on the gasket and possibly the temperatures at the sample and at the gasket differ. Therefore, the first measurement

Table 5 Lattice parameters of NiS at various temperatures

	T (°C)	a (Å)	c (Å)	V (Å^3)	c/a
Millerite	50	9.618(2)	3.1525(8)	252.57(9)	0.3278
	100	9.624(2)	3.1526(9)	252.86(9)	0.3276
	150	9.630(2)	3.156(1)	253.41(1)	0.3277
	200	9.641(2)	3.158(1)	254.2(1)	0.3276
	300	9.649(2)	3.1590(9)	254.69(9)	0.3278
	350	9.661(1)	3.1620(9)	255.57(8)	0.3276
	360	9.663(2)	3.1633(9)	255.79(8)	0.3274
	370	9.664(1)	3.1630(9)	255.81(8)	0.3273
	380	9.666(2)	3.161(1)	255.77(9)	0.3270
	390	9.663(2)	3.160(2)	255.6(1)	0.3270
	400	9.668(3)	3.163(4)	256.0(3)	0.3272
NiAs type	20	3.4375(7)	5.351(1)	54.69(2)	1.5549
	380	3.448(1)	5.385(2)	55.44(3)	1.5618
	390	3.4485(5)	5.3842(7)	55.45(1)	1.5613
	400	3.449(1)	5.389(2)	55.51(3)	1.5625
	450	3.4512(8)	5.394(1)	55.63(2)	1.5629

Fig. 6 Volumes per formula unit V_{fu} of millerite and NiAs-type NiS at high temperatures. The *lines* are guides to the eyes

Table 6 Comparison of interatomic distances in millerite and NiAs type NiS under ambient conditions

	Interatomic distances (Å)			
	Millerite		NiAs-type NiS	
$d_{(Ni-S)}$ (Å)	1x	2.266	6x	2.394
	2x	2.277		
	2x	2.362		
$d_{(Ni-Ni)}$ (Å)	2x	2.531	2x	2.676
$d_{(S-S)}$ (Å)	2x	3.151	6x	3.332
	2x	3.238	6x	3.440
	4x	3.355		
	4x	3.817		
averaged $d_{(S-S)}$ (Å)		3.456		3.386

was done with an unpressurized sample in the diamond-anvil cell. The measured transition temperature was 400 °C, about 20 °C higher than that determined in the experiments without a high-pressure cell. At 2.6 GPa the onset of the transformation occurred at 310 °C, and at 7.2 GPa the NiAs type was observed at only 230 °C. Probably, the true transition temperatures are also about 20 °C lower. The decrease of the transition temperature with pressure gives rise to the assumption that at higher pressures the NiAs type may already be formed at room temperature, but such a transition was not observed in our experiments up to 35 GPa.

Fitting a third-order Birch–Murnaghan equation-of-state, Campbell and Heinz (1993) yielded for NiAs-type NiS a bulk modulus of $K = 156(10)$ GPa with a pressure derivative $K' = 4.4(12)$. Figure 8 shows the pressure-dependent variations of the volume per formula unit of both modifications of NiS. Since millerite is more compressible at room temperature than the NiAs-type modification, it might be the stable phase at high pressure. It is assumed that there is a minimum value for the transition temperature at high pressure.
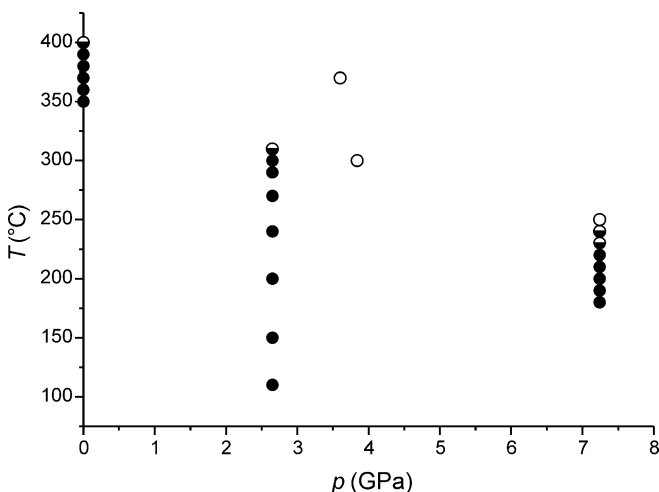
Fig. 7 Results of the high-pressure–high-temperature investigations. ● only millerite; ○ only NiAs-type NiS; ◐ both phases observed
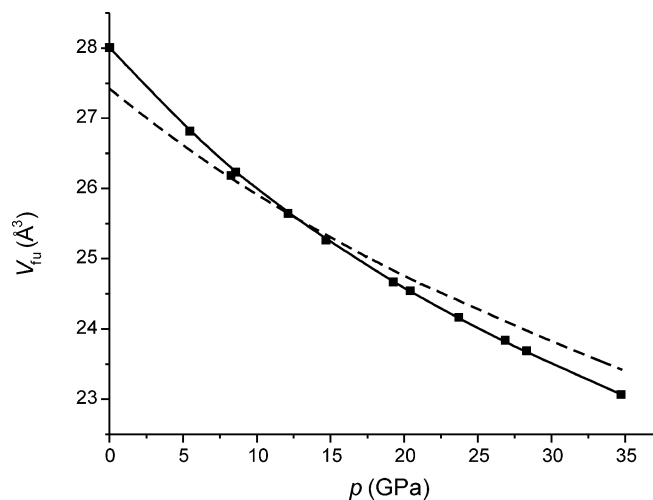
Fig. 8 Volumes per formula unit of millerite and NiAs-type NiS at high pressures V. Data of NiAs-type NiS Campbell and Heinz (1993). *Solid line* millerite; *dashed line* NiAs-type NiS

References

Ahsbahs H (1987) X-ray diffraction on single crystals at high pressure. Prog Crystal Growth Character 14: 263–302

Ahsbahs H (1995) 20 Jahre Merrill-Bassett-Zelle. Einige Neuheiten. Z Kristallogr Suppl 9: 42

Ahsbahs H (2001) Eine MB-Druckzelle, speziell zur Verwendung mit Flächenzählern. Z Kristallogr Suppl 18: 59

Ahsbahs H (2004) New pressure cell for single-crystal x-ray investigations on diffractometers with area detectors

Angel RJ (2002) EOSFIT, version 5.2. http://www.crystal.vt.edu/crystal/software.html

Campbell AJ, Heinz DL (1993) Equation of state and high-pressure phase transition of NiS in the NiAs structure. J Phys Chem Solids 54: 5–7

Finger LW, King HE (1978) A revised method of operation of the single-crystal diamond cell and refinement of NaCl at 32 kbar. Am Mineral 63: 337–342

Grice JD, Ferguson RB (1974) Crystal structure refinement of Millerite (β-NiS). Can Mineral 12: 248–252

King HE, Finger LW (1979) Diffracted beam crystal centering and its application to high-pressure crystallography. J Appl Crystallogr 12: 374–378

Krishnakumar SR, Shanthi N, Sarma DD (2002) Electronic structure of millerite NiS. Phys Rev (B) 66: 115105

Kullerud G, Yund RA (1962) The Ni–S system and related minerals. J Petrol 3:126–175

Kutoglu A (1995) CRYMIS. A computer software package for structural analysis. Univ Marburg

Mao HK, Xu J, Bell PM (1986) Calibration of the ruby pressure gauge to 800 kbar under quasi-hydrostatic conditions. J Geophys Res 91: 4673–4676

McWhan DB, Marezio M, Remeika JP, Dernier PD (1972) Pressure–temperature phase diagram and crystal structure of NiS. Phys Rev (B) 5: 2552–2555

Okamura H, Naitoh J, Nanba T, Matoba M, Nishioka M, Anzai S, Shimoyama I, Fukui K, Miura H, Nakagawa H, Nakagawa K, Kinoshita T (1999) Optical study of the metal-nonmetal transition in $Ni_{1-\delta}S$. Solid State Comm 112: 91–95

Piermarini GJ, Block S, Barnett JD, Forman RA (1975) Calibration of the R_l ruby fluorescence line to 195 kbar. J Appl Phys 46: 2774–2780

Rajamani V, Prewitt CT (1974) The crystal structure of millerite. Can Mineral 12: 253–257

Ralph RL, Finger LW (1982) A computer program for refinement of crystal orientation matrix and lattice constants from diffractometer data with lattice symmetry constraints. J Appl Crystallogr 15: 537–539

Raybaud P, Hafner J, Kresse G, Toulhoat H (1997) Ab initio density functional studies of transition-metal sulphides. II. Electronic structure. J Phys Condens Matter 9: 11107–11140

Sheldrick GM (1993) Program SHELXL-93. Program for the refinement of crystal structures. University of göttingen, Germany

Sowa H, Koch E and Fischer W (2003) Hexagonal and trigonal sphere packings. I. Invariant and univariant lattice complexes. Acta Crystallogs (A) 59: 317–326

Sparks JT, Komoto J (1963) Neutron diffraction study of NiS. J Appl Phys 34: 1191–1192

Trahan J, Goodrich RG, Watkins SF (1970) X-ray diffraction measurements on metallic and semiconducting hexagonal NiS. Phys Rev (B) 2: 2859–2862

Vuorelainen Y, Huhma A, Häkli A (1964) Sederholmite, wilkmanite, kullerudite, mäkinenite and trüstedtite, five new nickel selenide minerals. Bull Comm Geol Finlande 215: 113–126

Zhang L, Ahsbahs H (1998) New pressure domain in single-crystal X-ray diffraction using a sealed source. Rev High Pressure Sci Technol 7: 145–147